Pergamon

Journal of Structural Geology, Vol. 16, No. 4, pp. 505 to 517, 1994

0191-8141/94 $6.00+0.00

0191-8141(93)E0016-E

Primary fabric ellipsoids in sandstones: implications for depositional processes and strain analysis

SCOTT R. PATERSON and HAO YU

Department of Geological Sciences, University of Southern California, Los Angeles, CA 90089-0740, U.S.A.

(*Received* 25 *January* 1993; *accepted in revised form* 23 *November* 1993)

Abstract—When measuring strains in deformed clastic rocks, geologists usually assume one or more of the following: (1) objects were initially circular; (2) objects were initially non-circular but had uniform orientations; (3) object populations initially had a fabric, but that this fabric had a symmetrical relationship to bedding; or that (4) initial fabrics are recognizable even after straining. To evaluate these assumptions, we measured 43 fabric ellipsoids in non-strained, poorly sorted sandstones from four depositional settings: DSDP core 174 (fan and abyssal plain deposits off the coast of Oregon); the Cretaceous Great Valley sequence, California (fore-arc deposits); the Cretaceous Pigeon Point Formation, California (accreted and slumped turbidites); and cross-bedded sandstones from intracontinental basins in California and Australia. Our results indicate the following: (1) in two-dimensional cuts, individual grains have variable but usually small axial ratios (<3/1) and grains with larger axial ratios are more often, but not always, oriented at small angles to bedding; (2) averaged ratios and orientations of populations of grains in three dimensions define non-spherical fabric ellipsoids, but with small axial ratios (average principal ratios = 1.31:1.14:1); (3) these fabric ellipsoids show a wide range of shapes; and (4) orientations of fabric ellipsoid XY planes have highly variable orientations and are not parallel to bedding or cross-bedding. These results indicate that fabric ellipsoids measured in deformed sandstones must be corrected for the presence of primary fabrics when attempting to calculate strains. However, because of the variable orientations and shapes of the primary fabric ellipsoids and lack of relationship to bedding, strains can, at best, only be bracketed by multiplying final ellipsoids measured in strained samples by reciprocal primary fabric ellipsoids having a variety of orientations and shapes.

These data and microstructures in grains and matrix cements also argue against significant compaction during burial in these clast-supported, sand-rich units and instead suggest that the primary fabrics largely reflect grain packing processes during deposition, and/or slumping and packing in the case of the Pigeon Point samples.

INTRODUCTION

GRAIN preferred orientations (GPOs) and grain shapes have long been used to make inferences about the nature of depositional and post-depositional sedimentary processes in sandstones such as compaction and slumping. GPOs have also been used to estimate the amount of distortion (strain) during post-lithification tectonism, and along with microstructural analyses, to determine the deformation mechanisms by which this strain occurred. Such studies are rarely linked, however: sedimentologists look at grain shapes or grain orientations but rarely use techniques to combine the two types of data as is routinely done by structural geologists. In turn, structural geologists usually make assumptions about the nature of GPOs and grain shapes in non-strained sandstones when evaluating strains and microstructures in deformed rocks. The most common assumptions are the following: (1) objects were initially circular; (2) objects were initially non-circular but had random (or uniform) orientations; (3) object populations initially had a fabric, but that this fabric had a symmetrical relationship to bedding; or that (4) the effect of initial fabrics are recognizable even after straining.

In this study, we examine GPOs, grain shapes and microstructures in non-strained (on hand sample scale) sandstones from a variety of depositional settings (Fig. 1): (a) samples from Deep Sea Core 174A located off the coast of Oregon; (b) samples from the Great Valley sequence, California (GVS); (c) samples from the Pigeon Point Formation, California; and (d) miscellaneous cross-bedded sandstones from continental basins in California and Australia. These data will be used to evaluate depositional and post-depositional processes in these sandstones as well as implications for studies of strain and deformation mechanisms in their deformed equivalents.

We emphasize that all samples analyzed in this study show no cleavage, no evidence of post-lithification pressure solution or crystal-plastic deformation, only rarely have transgranular fractures and veins, and are class-supported sandstones with non-deformed cements (except for the poorly lithified DSDP samples). We therefore argue that the measured fabrics reflect primary (pre-lithification) fabrics.

SAMPLE LOCALITIES, PREPARATION AND PETROLOGY

Deep Sea Core 174A

This core, drilled in the distal portion of the Astoria Fan off the coast of Oregon (Figs. 1 and 2) and now stored at Scripps Institute, San Diego, California, reached 879 m below the sea floor and recovered rocks from two units: (1) Upper Pleistocene thick- to thin-bedded, medium to fine turbiditic sands consisting of

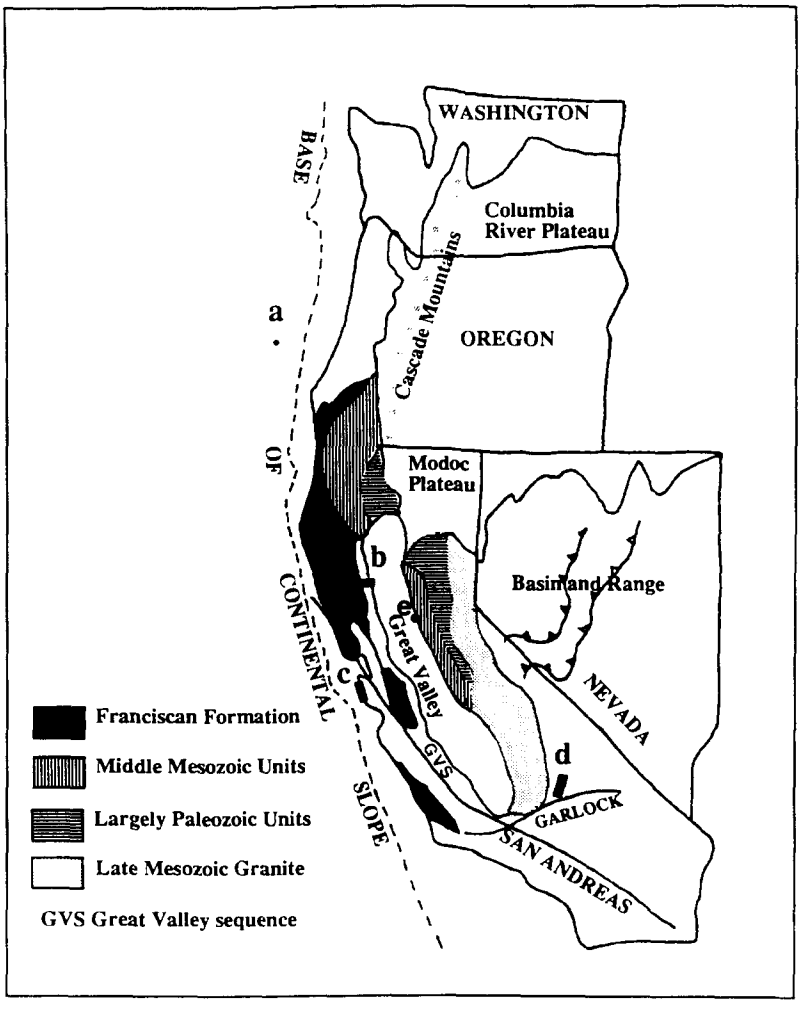

Fig. 1. Location map of sampled areas with respect to west coast of the United States. a shows the location of DSDP core 174A; b shows the location of Great Valley samples; c gives the location of Pigeon Point samples; d gives the location of Dove Springs samples; and e gives the location of Ione samples.

continental detritus deposited in the Astoria fan (0–284 m); and (2) the underlying Plio-Pleistocene thin-bedded sands, silts and clays (284–879 m) representing abyssal plain deposits (Kulm *et al.* 1973). This drill site is located seaward of the toe of the accretionary prism (Fig. 2).

Ten samples were collected from the core, three of which had to be discarded during preparation and analysis (Table 1). Each sample was oriented with respect to the vertical axis of the core, impregnated, and three oriented, mutually perpendicular thin sections constructed. During DSDP coring, an unknown amount of rotation around the vertical core axis occurred in these samples. Thus orientation data can only be measured with respect to horizontal. The preservation of horizontal bedding, laminations and other sedimentary structures (Kulm *et al.* 1973, Lundberg & Moore 1986) indicates that significant disruption of these samples did not occur during coring or sample preparation.

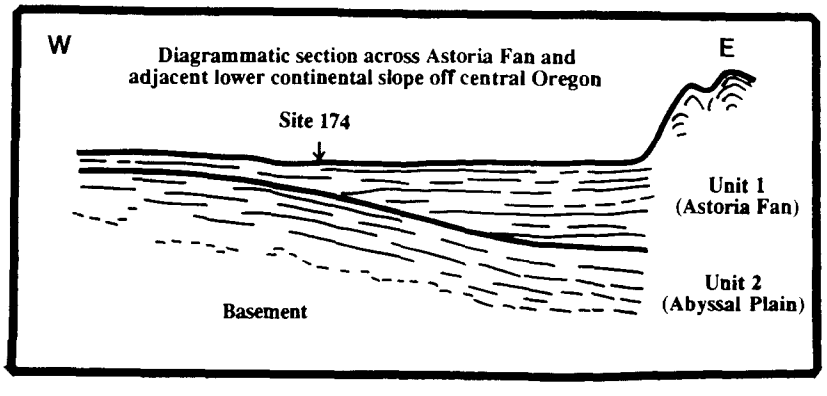

Fig. 2. Cross-section of Deep Sea Drill site 174A showing fan and abyssal plain deposits intersected by this core and toe of accretionary wedge to west. Figure redrafted from Kulm *et al.* (1973).

Table 1. Primary fabric ellipsoid data measured in sandstones. Apparent extensions assume that the final axial ratios (X, Y, Z) formed by constant volume strain of an initially perfectly uniform population of markers. SI = strain (or fabric) intensity and LP = Lode's parameter (negative numbers = prolate shapes, 0.0 = plane strain, positive numbers = oblate shapes). Equations given in Ramsay & Huber (1983). Right-hand column = angle measured between pole to bedding and pole to XY plane of fabric ellipsoids. ND = no data available

	Fabric ellipsoid axial ratios			Apparent extensions (%)			Strain intensity	Lode's parameter	Angle between bedding and
	X	Y	Z	X	Y	Z	SI	LP	XY plane
Deep Sea Core									
DS1	1.18	1.11	1.0	7.80	1.29	−8.42	0.12	0.24	28
DS4	1.31	1.06	1.0	17.39	−4.80	−10.52	0.20	−0.54	49
DS5	1.19	1.06	1.0	9.81	−1.57	−7.49	0.12	−0.28	44
DS7	1.25	1.18	1.0	9.52	3.80	−12.03	0.16	0.51	66
D8	1.35	1.18	1.0	15.81	0.73	−14.28	0.21	0.07	72
DS10	1.18	1.06	1.0	9.44	−1.72	−7.02	0.12	−0.32	88
DS11	1.25	1.20	1.0	8.90	5.06	−12.60	0.17	0.67	42
Pigeon Point									
1	1.50	1.20	1.0	23.31	−1.35	−17.79	0.29	−0.10	5
2	1.23	1.07	1.0	12.24	−2.36	−8.75	0.15	−0.35	28
3	1.13	1.06	1.0	6.40	−0.19	−5.84	0.09	−0.05	20
4	1.17	1.08	1.0	8.22	−0.10	−7.50	0.11	−0.02	56
5	1.24	1.05	1.0	13.56	−3.84	−8.42	0.16	−0.55	19
6	1.15	1.03	1.0	8.69	−2.65	−5.49	0.10	−0.58	33
7	1.18	1.17	1.0	5.97	5.07	−10.19	0.13	0.90	35
8	1.31	1.16	1.0	13.94	0.90	−13.02	0.19	0.10	16
9	1.30	1.16	1.0	13.36	1.16	−12.80	0.19	0.33	86
10	1.27	1.17	1.0	11.29	2.53	−12.37	0.17	0.31	52
Great Valley									
GVS1	1.97	1.34	1.0	42.54	−3.04	−27.64	0.48	−0.14	ND
GVS3	2.17	1.43	1.0	48.77	−1.96	−31.44	0.55	−0.08	ND
GVS5	1.27	1.02	1.0	16.50	−6.43	−8.27	0.19	−0.83	ND
GVS7	1.40	1.10	1.0	21.23	−4.75	−13.40	0.25	−0.43	ND
GVS9	1.81	1.34	1.0	34.72	−0.27	−25.57	0.42	−0.01	ND
GVS11	1.44	1.13	1.0	22.43	−3.93	−14.98	0.26	−0.33	ND
GVS13	1.44	1.13	1.0	22.43	−3.93	−14.98	0.26	−0.33	ND
GVS15	1.39	1.25	1.0	15.62	3.98	−16.82	0.24	0.36	ND
GVS20	1.30	1.20	1.0	12.30	3.24	−13.75	0.19	0.36	63
GVS21	1.18	1.10	1.0	8.40	0.51	−8.21	0.12	0.09	20
GVS22	1.18	1.03	1.0	10.30	−3.18	−6.36	0.12	−0.59	34
GVS24	1.09	1.02	1.0	5.38	−1.76	−3.41	0.07	−0.61	51
GVS26	1.27	1.14	1.0	12.60	0.40	−11.54	0.17	0.05	20
GVS28	1.08	1.04	1.0	3.80	0.14	−3.80	0.05	0.06	52
GVS29	1.18	1.13	1.0	6.90	3.00	−9.18	0.12	0.43	31
GVS31	1.23	1.15	1.0	9.49	2.44	−10.84	0.15	0.35	ND
GVS33	1.17	1.09	1.0	7.44	0.54	−7.68	0.11	0.10	33
GVS35	1.15	1.16	1.0	4.53	5.16	−9.03	0.12	1.09	35
Cross-bedded									
AUS	1.11	1.10	1.0	3.79	2.85	−6.33	0.08	0.82	ND
RR1	1.24	1.09	1.0	12.50	−1.70	−9.57	0.16	−0.24	70
RR2	1.11	1.09	1.0	4.45	2.01	−6.15	0.08	0.56	76
RR3	1.31	1.27	1.0	10.21	7.51	−15.61	0.21	0.81	60
RR4	1.15	1.07	1.0	7.38	−0.18	−6.71	0.10	−0.04	53
Io-1	1.19	1.16	1.0	6.88	4.18	−10.19	0.13	0.71	ND
Io-2	1.94	1.43	1.0	38.07	1.77	−28.83	0.47	0.08	ND
BD-1	1.19	1.08	1.0	9.45	−0.67	−8.02	0.12	−0.12	ND

Great Valley sequence

Eighteen oriented samples of sandstones and siltstones were collected from a transect through the Cretaceous Great Valley sequence, California, in the Wilbur Springs Quadrangle (Fig. 3). These interbedded sandstones, siltstones and shales represent proximal and distal, fore-arc fan sequences that after lithification have been tilted, and locally deformed by bedding parallel faults (Ingersoll 1979, Glen 1990). However, at least in the sampled area, the sandstones and siltstones are not cleaved and show no microstructural evidence of crystal-plastic strain. The orientation of bedding and other sedimentary structures were recorded, and three oriented, mutually perpendicular thin sections constructed from each sample.

Pigeon Point Formation

The Upper Cretaceous Pigeon Point Formation (Fig. 4) consists of turbiditic sequences of sandstone, siltstone, mudstone and local conglomerate (Hall *et al.* 1959, Wentworth 1960, Tyler 1972). Howell & Joyce (1981) divided the Pigeon Point Formation into various facies, of which facies F is characterized by abundant

(a)

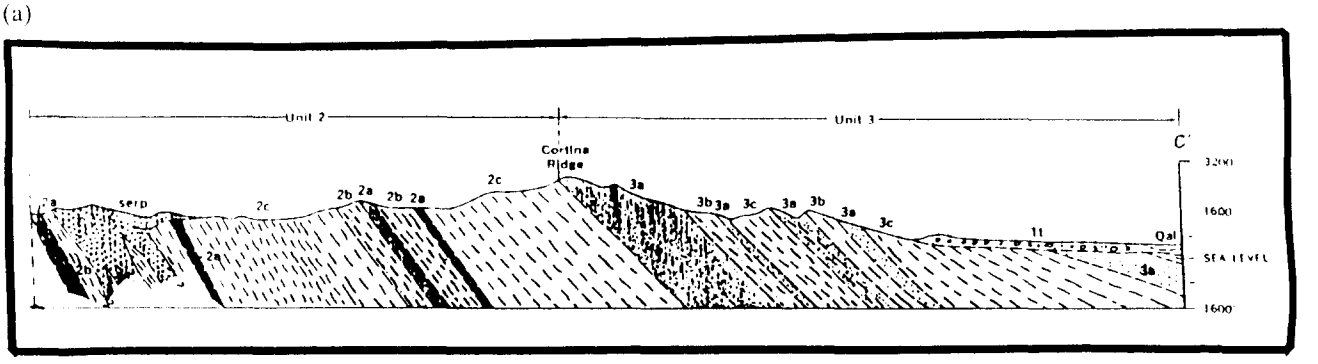

(b)

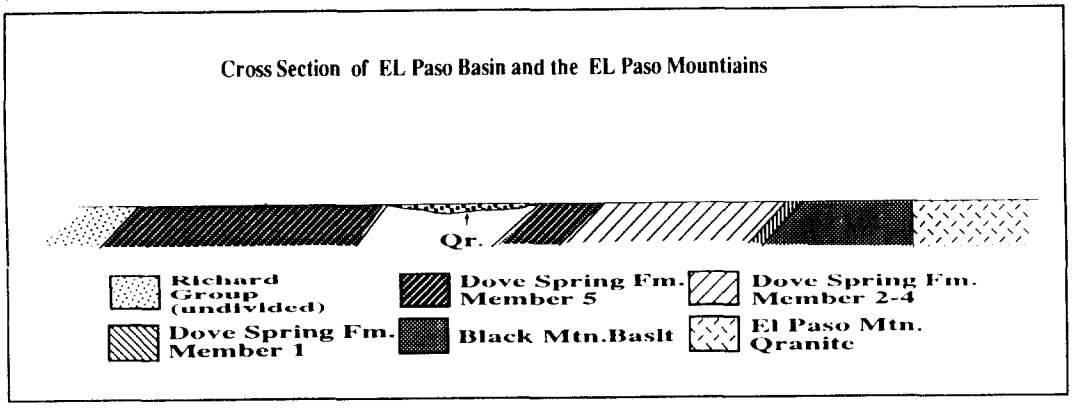

Fig. 3. Cross-sections through (a) the Great Valley sequence exposed in the Wilbur Springs Quadrangle, and (b) the El Paso Basin where the Dove Spring Formation is located. Cross-sections show the general homoclinal nature of each section as well as the amount of tilting.

slump structures. This facies consist of silt and sand distal turbidites with local, discontinuous mudstone and conglomerate layers. Siltstone consists of about 50% quartz, 10–20% feldspar and variable amounts of micas, chlorite and clays. Organic material makes up a small but visible part in many samples, and some organic-rich layers are present. The sandstones are immature with quartz the dominant mineral, although in some layers, the volume of feldspar and volcanic fragments is significant.

Although these rocks have been tectonically deformed by open, upright, regional-scale folds and brittle faults (Howell & Joyce 1981, Joyce 1981), metamorphic tectonites have not developed (Paterson & Tobisch 1993), and the following observations indicate that the fabrics described below formed by penecontemporaneous slumping (e.g. Tobisch 1984): (1) the isolated stratigraphic occurrence of deformed horizons; (2) truncation of folds by bedding and by non-deformed burrows and sand dikes; (3) truncation of slumped beds by locally developed faults that do not deform clastic grains or matrix cements; and (4) lack of evidence for metamorphism or crystal-plastic strain, although the layers clearly flowed during folding.

Ten oriented samples have been collected from outcrops of facies F along a beach immediately south of Pigeon Point and three, oriented, perpendicular thin sections prepared from each sample. The relationship between these samples and slumps, and structural data for these slumps are presented by Paterson & Tobisch (1993).

Miscellaneous sands

We have collected eight oriented samples of sandstones from four intracontinental, non-strained formations in California and Australia. These include one sample from well-sorted, medium-grained, cross-bedded, quartz-rich, Permian sandstone exposed in the Sydney basin, Australia, four samples from the coarse-grained, volcanic-rich sandstones from the upper Miocene Dove Spring Formation exposed north of Los Angeles, California (Fig. 1), two samples from the Eocene Ione Formation exposed west of Mariposa, California, and one from an unnamed Tertiary basin in the Mojave desert, California. All of these sandstones formed in continental basins and were sampled where cross-bedding was present. For each sample, the orientation of bedding and cross-bedding was recorded and three, oriented, mutually perpendicular thin sections prepared.

Petrology

Except for the miscellaneous sandstones, the samples all consist of 50–75% quartz, 10–20% feldspar and

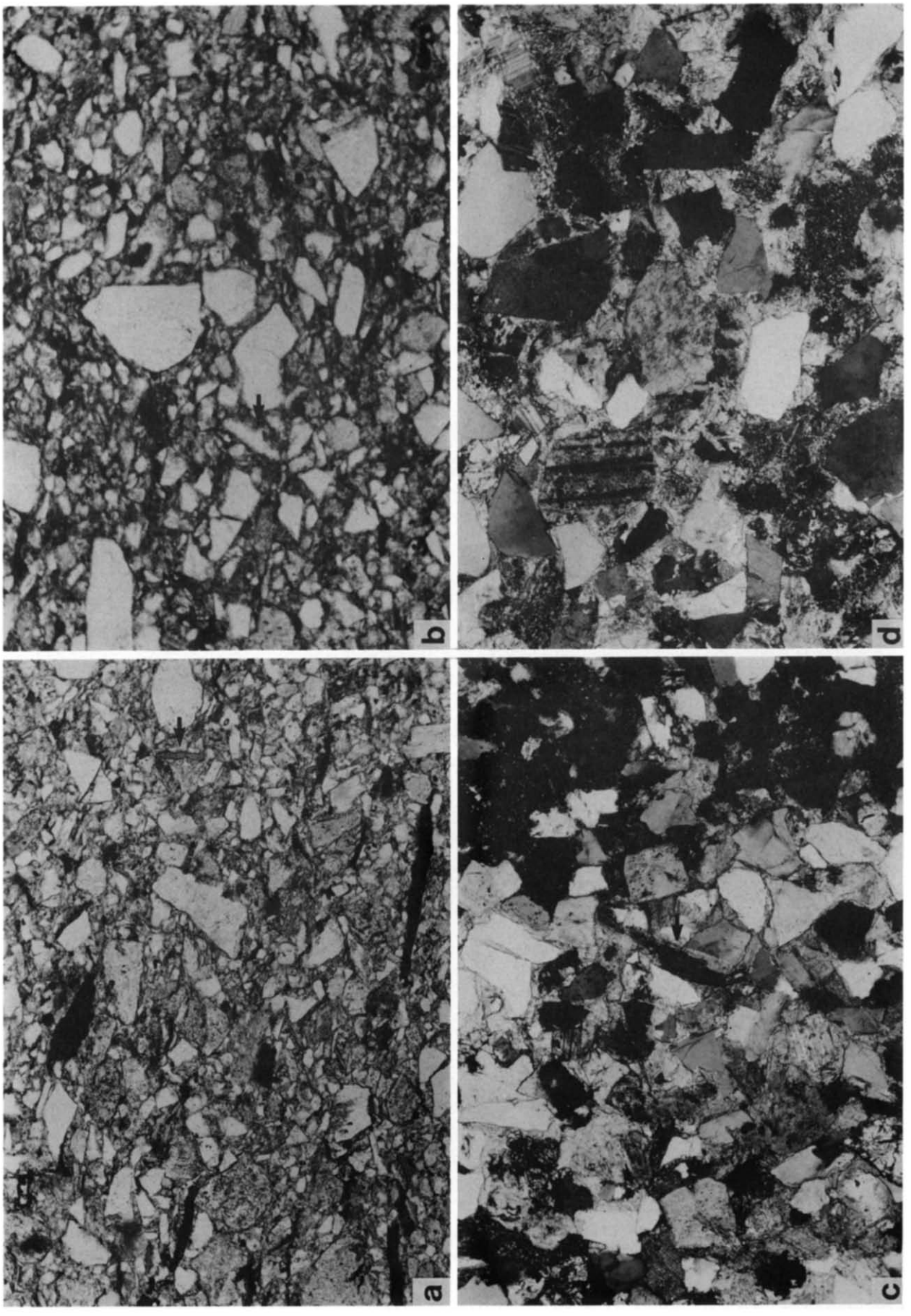

Fig. 5. Microstructures of sandstones (width of all photographs approximately 5 mm). (a) Pigeon Point Formation; (b) Great Valley sequence; (c) & (d) Dove Spring area. Bedding roughly horizontal in each photograph. Note the stronger alignment of opaques and detrital micas parallel to bedding in (a) and (b). Small black arrows point to detrital mica (a) or grains of quartz (b), (c) and (d) with long axes at high angles to bedding, although more often these grains have long axes at low angles to bedding. Most sand-sized grains show some undulose extinction and sometimes visible subgrains. Plagioclase and volcanic fragments often altering to sericite (e.g. c & d).

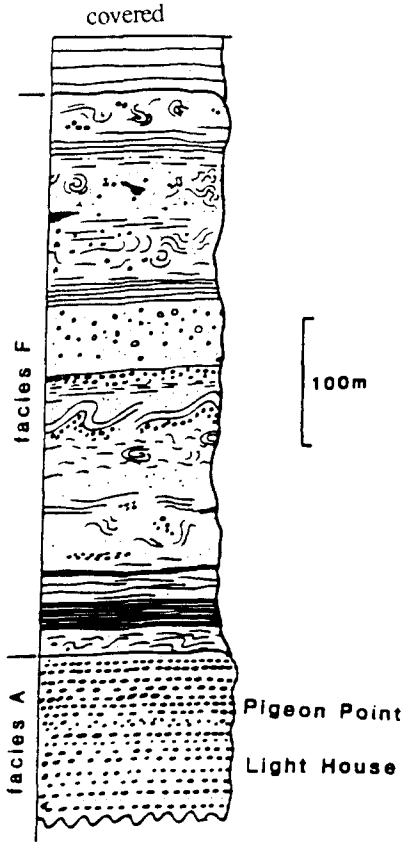

Fig. 4. Stratigraphic column of the sampled part of the Pigeon Point Formation (redrafted from Howell & Joyce 1981).

lesser, but variable, amounts of detrital micas and clays. Organic material makes up a small but visible part in many samples. Most grain sizes fall within the sand range, but 10–20% are silt size and a few percent are grit to conglomerate size. Thus these samples all reflect poorly sorted, clast-supported, arc-derived greywackes.

The petrology and clast size are more variable in the miscellaneous sands. Samples from the Dove Spring Formation are coarse sands to conglomerate and dominated by volcanic clasts. The Ione Formation samples are coarse-grained quartz dominated sands with some grit and pebble-sized fragments of variable compositions. The Sydney Basin sample is a mature, quartz-rich sandstone. Thus, these are also clast-supported sandstones, although the clast composition and degree of sorting varies from those described above.

In all samples individual sand grains (quartz and feldspar) tend to be roughly elliptical or rectangular in shape, but in detail their margins are often angular (Fig. 5). Quartz grains commonly show undulose extinction and some subgrain development and feldspar show both growth and deformation twins and minor alteration to sericite. However, these intracrystalline microstructures occur in grains from unlithified DSDP cores and in lithified samples in grains surrounded by non-deformed cements and are clearly inherited microstructures (Bennet *et al.* 1991; see also Fig. 5). Some intracrystalline fractures and other evidence of grain breakage exists, although evidence of this is not widespread. We also see no extensive inter-grain fractures or other features such as diffusion mass transfer or crystal plasticity (cf. Knipe 1986) in these sand-rich units that might suggest deformation of grains after lithification (Borradaile 1981, Bennet *et al.* 1991).

CALCULATION OF FABRIC ELLIPSOIDS

Grain populations consisting of variously shaped and oriented ellipsoidal objects can be represented by a fabric ellipsoid with three principal axes, $X > Y > Z$ (Elliott 1970, Shimamoto & Ikeda 1976, Wheeler 1986). In this study, fabric ellipsoids were calculated in the following manner. For each thin section, the long and short axis and orientation of the long axis of 50 or more grains were measured using an x–y digitizing microscope or image processing system (both data collection techniques gave identical results) and the data fed directly into computer data files. Average two-dimensional ellipses for each thin section were calculated using the algebraic method of Shimamoto & Ikeda (1976). Three-dimensional ellipsoids are calculated from the three, perpendicular, two-dimensional ellipses using the techniques of Shimamoto & Ikeda (1976) and Miller & Oertel (1979). When appropriate (i.e. if geographic orientations of samples are available) three-dimensional ellipsoids are reoriented to geographic co-ordinates. Because of uncertainties in the amount of vertical axis rotation of samples from DSDP cores and the different amounts of tilting of the lithified samples, a more useful measurement for this study is the relationship between the orientation of the XY principal plane of the calculated fabric ellipsoid and nearby bedding or cross bedding (Table 1, column 10).

These fabric ellipsoids represents the average shape and orientation of all measured grains. De Paor & Kusky (1988) noted that this method of representing grain populations may fail if enveloping surfaces of grain orientation and ratio plots are not ellipsoidal. However, this possibility can be checked by resectioning samples along planes 45° to the previous cuts and recalculating the fabric ellipsoid. Populations with roughly ellipsoidal enveloping surfaces should give identical fabric ellipsoids within the range of measurement errors. We recut and reanalysed two samples to evaluate the reproducibility of these three-dimensional ellipsoids. Within standard errors the results are identical indicating that the above technique appears acceptable for this study.

Two-dimensional results

Axial ratios of most individual grains vary between 1.0 and 3.0, although grains with ratios in excess of 10/1 exist. No strong preferred alignment of quartz or feldspar grains with axial ratios less than 3/1 is apparent in thin section (Fig. 5) nor when axial ratios and orientations are measured (Fig. 6). Long axes of grains with larger axial ratios also have variable orientations, although these grains are more likely to have their long axes at low angles to bedding (Fig. 5). Detrital micas and

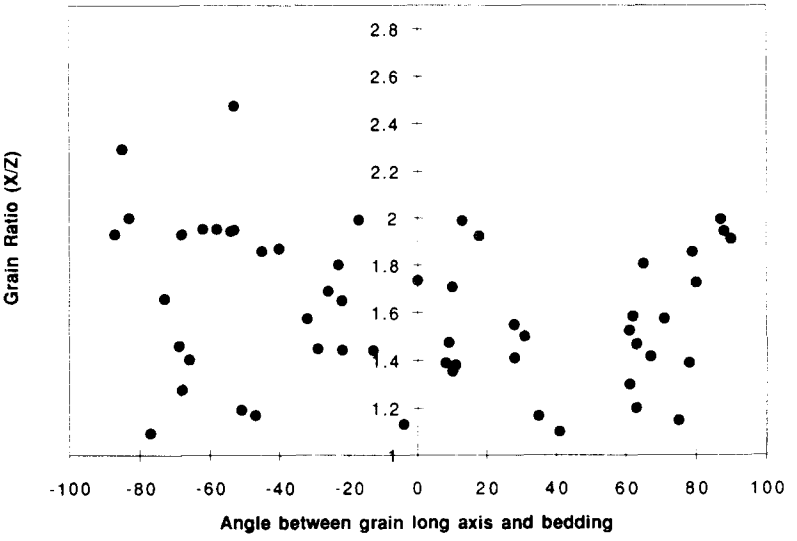

Fig. 6. Plot of grain ratios vs angle between bedding and grain long axis. Note that there is no systematic relationship between orientations of grains with respect to bedding for grains with moderate to small ratios (ratios < 2.6 in this sample).

phyllosilicate grains also show variable orientations, although there is often a weak preferred orientation parallel to bedding. We emphasize, however, that detrital micas or quartz grains with large axial ratios with long axes at high angles to bedding are not uncommon (Fig. 5). These quartz grains can be quite acicular and undeformed and the micas not kinked, providing textural evidence against significant post-depositional compaction in these sand-rich layers.

To evaluate the relationship between bedding and grain ratios and orientations, we examined thin sections which are perpendicular to bedding. Plots of the number of grains vs grain axial ratios and number of grains vs grain orientations (e.g. Figs. 7 and 8), show that grain orientations and grain ratios range from uniform to weak Gaussian distributions. Plots of grain axial ratios vs long axis orientations (R_f–theta plots) show typical tear-dropped shapes (Fig. 9) similar to those of weakly *deformed* grain populations (Lisle 1985).

Three-dimensional results

Three-dimensional principal axial ratios for calculated fabric ellipsoid are shown in Table 1 and orientations of the *XY* principal planes vs bedding are presented in Table 1 and Fig. 10. We also have used these principal axial ratios to calculate apparent (since these ellipsoids do not reflect strain) constant volume extensions, strain intensities (SIs), and Lode's parameters (LPs) as is commonly done when measuring strains in deformed sandstones. The fabric ellipsoids are also plotted on a Flinn diagram (Fig. 11) for comparison with similar plots of data from deformed samples (e.g. Ramsay & Huber 1987).

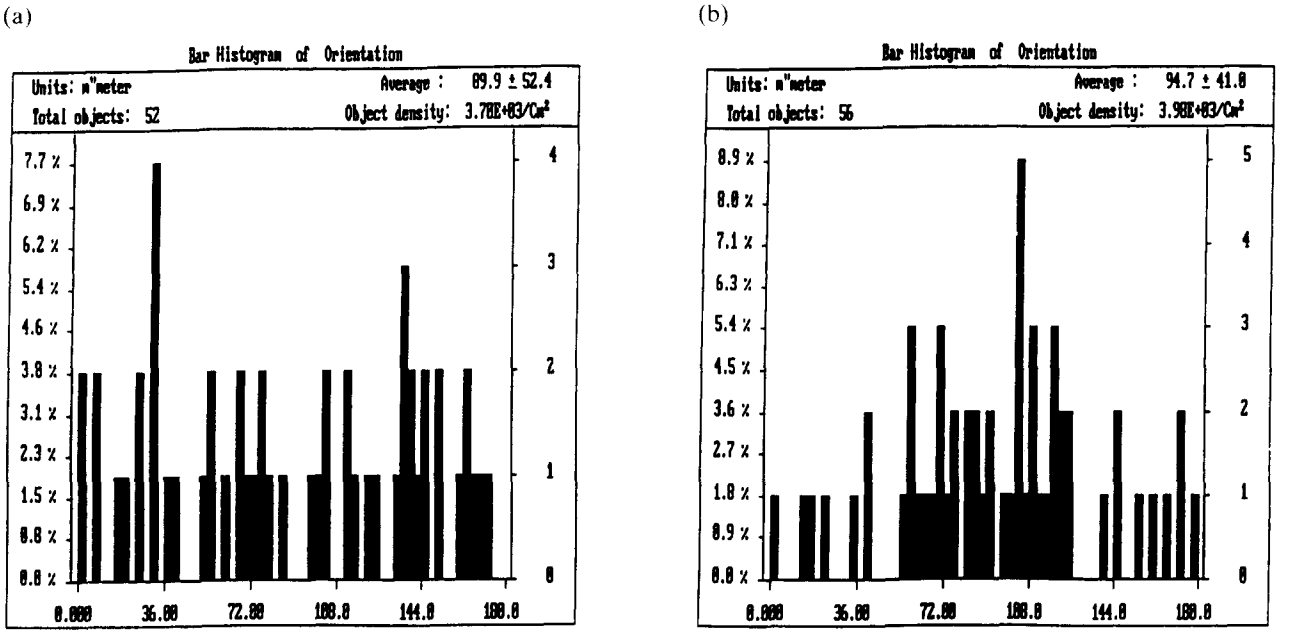

Fig. 7. Bar histograms of orientations of grain long axes showing a uniform distribution (a) to weak Gaussian distribution (b). Sample size = total objects.

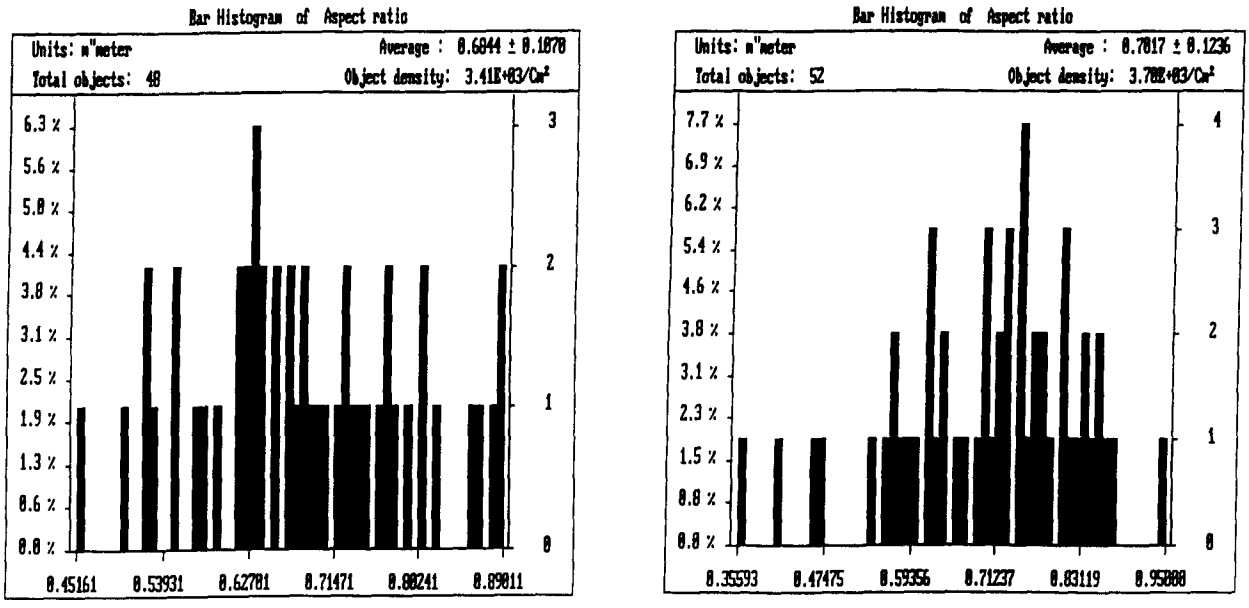

Fig. 8. Bar histograms of grain ratios (long/short axes) showing uniform distributions (a) to weak Gaussian distributions (b). Sample size = total objects.

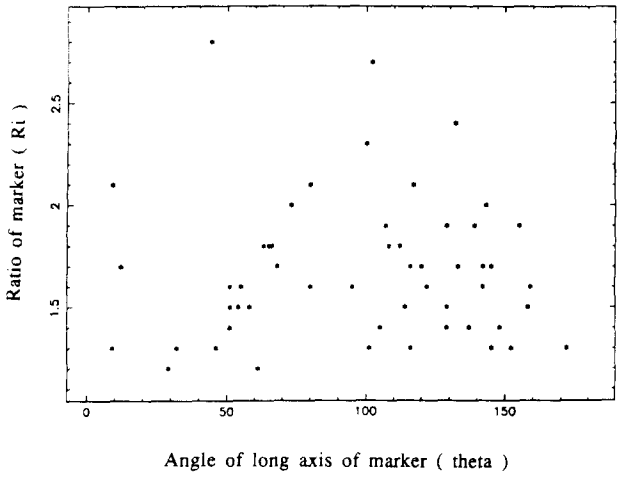

Fig. 9. Plot of grain ratios vs grain orientations (i.e. R_i–theta plot). Note weak preferred orientation of grains defined by tear-dropped shape of data centered around orientation of 100°.

The orientation of the fabric ellipsoids show no strong relationship to cross-bedding, only a weak tendency for XY principal planes to be close to bedding, and in fact, have a surprisingly wide range of orientations (Table 1, column 10). Ellipsoid shapes also vary widely from prolate (constrictional) to oblate (flattening) shapes (Table 1 and Fig. 11). As indicated by calculated ellipsoid SIs (Table 1), which fall between 0.05 and 0.55, or K values on the Flinn plot (Fig. 11) which fall between 0.8 and 0.25, ellipsoids do not cluster around the origin of the Flinn diagram as is commonly assumed for non-deformed sandstones.

Information is available about depths of burial for the samples from the DSDP core and from the Great Valley sequence. Plots of ellipsoid orientation vs depth, ellipsoid SI vs depth and LP vs depth show no systematic relationship between these data and depth (e.g. Fig. 12).

SUMMARY AND CONCLUSIONS

We argue that the fabric ellipsoids calculated in this study largely reflect depositional processes for the following reasons: (1) the lack of microstructural evidence that any of the samples underwent penetrative deformation after deposition (DSDP samples) or lithification; (2) the observation that these fabric ellipsoids occur in unlithified DSDP cores and in lithified samples with nonstrained cements; and (3) the lack of any relationship between the size, shape, or orientation of calculated fabric ellipsoids and small- or large-scale tectonic structures. We also argue that significant compaction (vertical shortening of units during burial) did not occur after deposition of these samples because for the following reasons: (1) the presence of non-deformed acicular quartz grains and non-deformed detrital micas with long axes at high angles to bedding; and (2) lack of any strong relationship between fabric ellipsoid orientations and bedding, and between ellipsoid orientation, shape, size and depth of burial. If compactions did occur, they must have done so without strongly affecting the geometrical arrangement of the quartz grains.

Some information is available about depositional flow directions for the Great Valley sandstones (Ingersoll 1970) and slump directions for the Pigeon Point samples (Tobisch 1984). X axes of the calculated fabric ellipsoids are not strongly aligned parallel to these directions, although more occur at low angles than high angles to these directions. We therefore argue that the measured fabric ellipsoids reflect grain shapes inherited from erosional histories and grain orientations controlled by packing during deposition of a large number of grains with low axial ratios and that flow, or later slumping (e.g. Pigeon Point samples), only had a mild influence. That is, during deposition, the orientation of individual grains will be controlled by its interaction with pre-

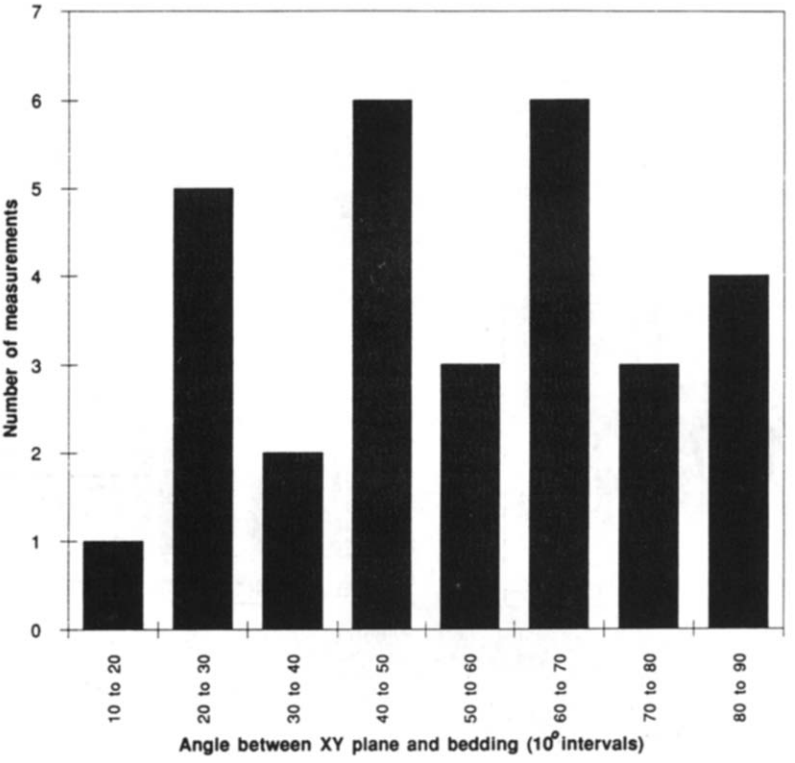

Fig. 10. Histogram showing angle between *XY* plane of fabric ellipsoid and bedding. Note that there is no systematic relationship between the orientations of the fabric ellipsoids and bedding.

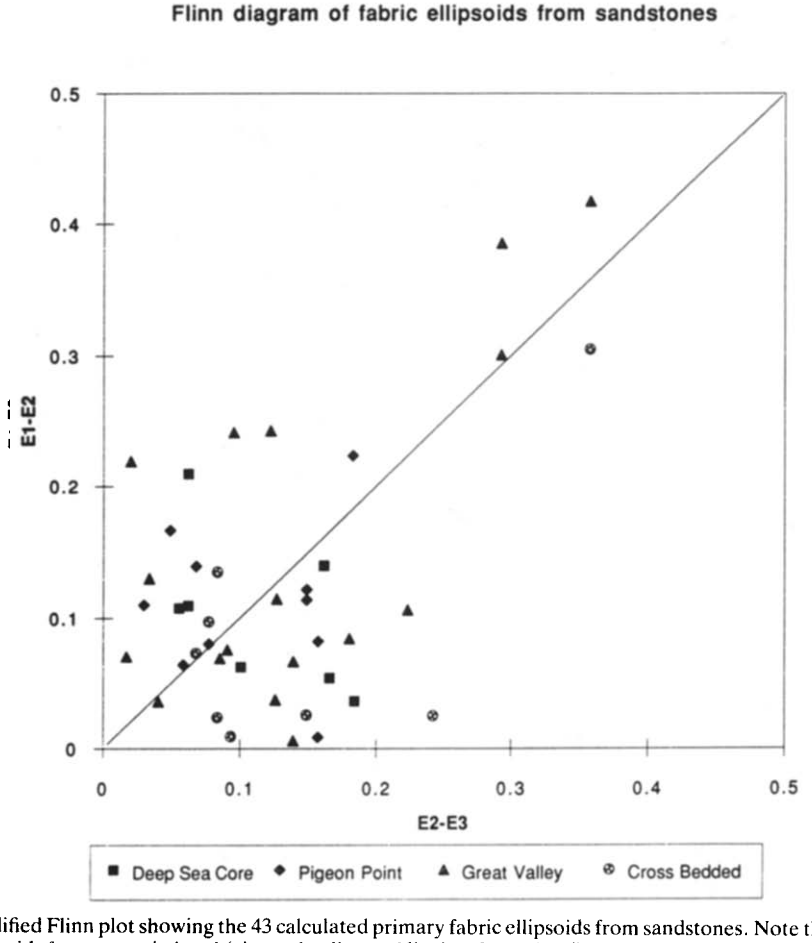

Fig. 11. Modified Flinn plot showing the 43 calculated primary fabric ellipsoids from sandstones. Note the wide variation in shape of ellipsoids from constrictional (above the diagonal line) to flattening (below diagonal line). Note also that ellipsoids do not cluster at origin indicating that fabrics are not perfectly uniform.

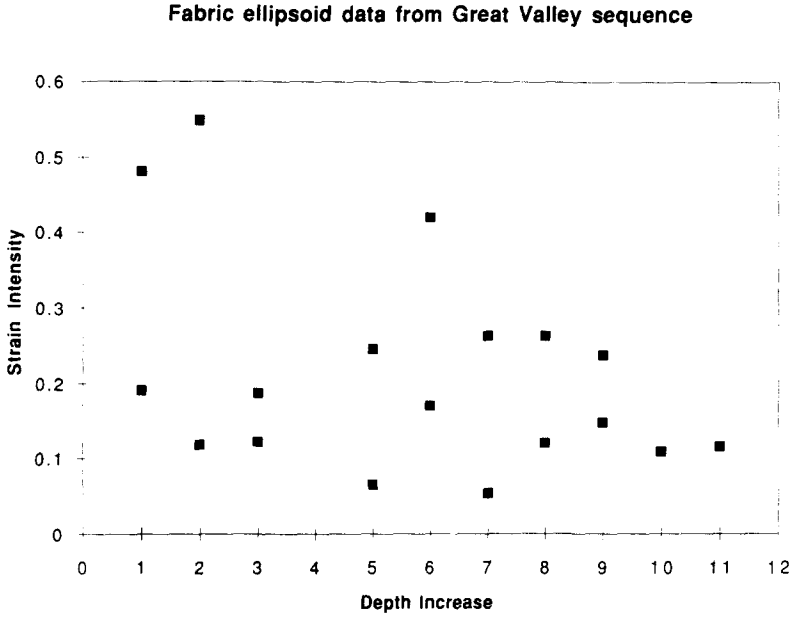

Fig. 12. Plot of strain intensity vs burial depth for sandstones from Great Valley sequence. Depth increments approximately 100 m increments below the shallowest measured unit. An unknown additional amount of now eroded material was above this highest unit. Note that fabric intensities do not increase with increasing depth of burial.

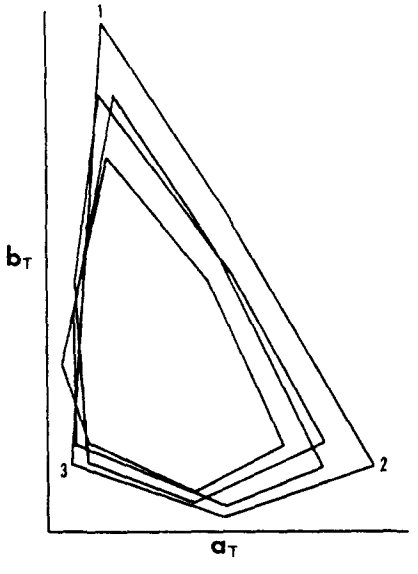

Fig. 13. Diagram redrafted from Ramsay (1967) showing fields on a modified Flinn diagram of possible combinations of two ellipsoids. Note that the fields are roughly triangular in shape with three extreme points. These points represent three of the possible six ways to coaxially combine two ellipsoids. Axes same units as in Fig. 11 but with arbitrary distances.

viously deposited grains. Acicular quartz grains with larger axial ratios do show a stronger alignment parallel to bedding and to flow directions. Detrital micas show the strongest alignment, although both the acicular quartz grains and micas still have highly variable orientations, some which have ended up with long axes at high angles to flow directions.

Our data also show that three of the assumptions made during strain analyses of sandstones are incorrect: (1) individual grains are not spherical prior to straining; (2) orientations and shapes of grain populations do not define spherical, pre-strain fabric ellipsoids (i.e. grains do not have an initial uniform distribution); and (3) pre-strain fabric ellipsoids are not symmetric around bedding (see also Boulter 1976). We also argue that the fourth assumption, that initial grain fabrics are recognizable after strain, is also unlikely in sandstones given the wide range in primary fabric ellipsoid shapes and orientations (Boulter 1976, Holst 1982).

Since these assumptions do not hold for sandstones, there are three important implications that need mentioning. First, any strain analysis in sandstones based on grain shapes and orientations where the resulting principal ratios are small (1.5 or less) may largely reflect depositional fabrics and thus must be carefully evaluated (e.g. Boulter 1976, Holst 1982, Yu & Paterson 1991). Second, *XY* planes of final fabric ellipsoids may not be parallel to foliations, except at large strains (strain ratios $\gg$3.0) where the two may become indistinguishable (Yu & Paterson 1991). Third, analysis of strain in sandstones must include a correction for the existence of primary fabrics since even slight deviations in the types of primary fabrics may lead to significant errors in strain calculations (e.g. Seymour & Boulter 1979).

Two-dimensional corrections for the removal of the effects of primary fabrics can be grouped into graphical procedures (e.g. Elliott 1970, Dunnet & Siddans 1971, Boulter 1976, Lisle 1977, De Paor 1988) and algebraic procedures (e.g. Oertel 1970, Matthews *et al.* 1974, Shimamoto & Ikeda 1976, Seymour & Boulter 1979, Holst 1982). However, all of these procedures makes one or more of the assumptions listed above and/or assume the existence of independent information about directions of principal axes of the strain ellipsoid. We therefore argue that none of these corrections are particularly valid.

Wheeler (1986) proposed an algebraic approach of factoring the final fabric ellipsoid into a tectonic strain

Table 2. Averaged data for primary fabric ellipsoids in different rock types (number of non-strained samples analyzed in parentheses). Other values same as in Table 1. Data reflect non-directed averages (see Oertel 1981). Some data for volcanic and accretionary lapilli from Tobisch *et al.* (1977). These axial ratios are what we presently use to bracket strain in deformed samples. See text for discussion

Average fabric ellipsoids in various rock types								
	Ratios			Apparent extensions (%)				
Rock types	*X*	*Y*	*Z*	*X*	*Y*	*Z*	Apparent SI	Apparent LP
Volcanic lapilli (17)	1.19	1.11	1	8	1	−9	0.12	0.20
Accretionary lapilli (4)	1.25	1.20	1	9	5	−13	0.17	0.63
Volcanic lahar (2)	1.25	1.15	1	11	2	−11	0.16	0.25
Conglomerate (5)	1.30	1.10	1	15	−2	−11	0.16	−0.29
Pebbly mudstone (2)	1.25	1.15	1	11	2	−11	0.16	0.25
Sandstone (43)	1.31	1.14	1	15	−3	−13	0.19	−0.03
Shale (14)	1.48	1.35	1	18	7	−21	0.29	0.52

ellipsoid superimposed on an initial fabric ellipsoid. He applied the method to an example that assumes a primary fabric ellipsoid with bedding as a symmetry plane. Since sandstone fabrics apparently rarely have bedding as a symmetry plane and information about primary fabric ellipsoid ratios and orientations is usually unknown, we suggest that in most cases the best one can do is to bracket strain by multiplying final measured ellipsoids by an average reciprocal primary fabric ellipsoids in the following manner: (1) principal axial ratios of the primary fabric ellipsoid can be calculated by determining a non-directed average (e.g. Oertel 1981) of multiple measured primary fabric ellipsoids (e.g. our average ratios = 1.31/1.14/1); (2) if information is available about primary fabric orientations, then a particular orientation can be used. If not, a range of orientations can be used as discussed below; (3) a reciprocal primary fabric ellipsoid is calculated using the above ratios and orientation(s); and (4) this reciprocal ellipsoid(s) and final measured ellipsoid are multiplied, the resulting ellipsoid representing an estimate of the strain ellipsoid (e.g. Wheeler 1986).

The largest uncertainty in this correction is the unknown orientation of the primary fabric ellipsoid in strained samples. But this problem may not be as bad as it first appears. Ramsay (1967) noted that all possible combinations of two ellipsoids fall within a roughly triangular region with three extreme points (Fig. 13). These extreme points reflect three of the six possible ways of coaxially combining two ellipsoids. Fortunately, because the principal axial ratios of primary fabric ellipsoids tend to be small (Tables 1 and 2), this triangular-shaped region tends to be relatively small when final ellipsoids are combined with primary fabric ellipsoids.

Thus our approach of attempting to bracket strains in tectonically deformed rocks is the following: (1) use GPOs and grain shapes to determine an ellipsoid in deformed rocks; (2) use GPOs and grain shapes to determine primary fabric ellipsoids in similar but non-deformed equivalents and calculate non-directed averages for each rock type (Table 2); (3) calculate reciprocal primary fabric ellipsoids using the average ratios in Table 2; and (4) coaxially combine the ellipsoid from the deformed rock and the reciprocal ellipsoid(s) in order to determine the three extreme points of the triangular region on the Flinn plot (Fig. 13). The actual value of strain is bracketed by these points.

We have a limited amount of data available on the nature of primary fabric ellipsoids in other rock types (Table 2). Although a detailed discussion of these data is beyond the scope of this paper, we list these data here for two reasons: (1) to emphasize that the existence of primary fabrics in non-strained rocks is widespread; and (2) to show the magnitude of axial ratios we presently use to bracket strains in our deformed samples. Clearly additional measurements of primary fabric ellipsoids in all rock types would be useful.

Acknowledgements—Acknowledgements are made to the Donors of The Petroleum Research Fund, administered by the American Chemical Society and to the Faculty Initiative Research Fund grant, University of Southern California for partial support of this research. We also thank Othmar Tobisch and Gerhard Oertel for discussions about strain and primary fabrics, and Tom Brudos, Mary Park and Tim Redfield for sample collection and help with measuring GPOs. We thank David Anastasio for a thorough review of the manuscript and Jack Henderson for editorial help.

REFERENCES

Bennet, R. H., Bryant, W. R. & Hulbert, M. H. 1991. *Microstructures of Fine-grained Sediments from Mud to Shale*. Springer, New York.

Borradaile, G. J. 1981. Particulate flow of rock and the formation of cleavage. *Tectonophysics* **72**, 305–321.

Boulter, C. A. 1976. Sedimentary fabrics and relation to strain-analysis methods. *Geology* **4**, 141–146.

De Paor, D. M. 1988. R_f/ϕ strain analysis using an orientation net. *J. Struct. Geol.* **10**, 323–334.

De Paor, D. G. & Kusky, T. M. 1988. Strain analyses in rocks with pretectonic fabrics: Discussion and reply. *J. Struct. Geol.* **10**, 529–532.

Dunnet, D. & Siddans, A. W. B. 1971. Non random sedimentary fabrics and their modification by strain. *Tectonophysics* **12**, 307–325.

Elliott, D. 1970. Determination of finite strain and initial shape from deformed elliptical objects. *Bull. geol. Soc. Am.* **81**, 2221–2236.

Glen, R. A. 1990. Formation of thrusting in some Great Valley rocks near the Franciscan Complex, California, and its implications for the tectonic wedging hypothesis. *Tectonics* **9**, 1451–1477.

Hall, C. A., Jones, C. L. & Brooks, S. A. 1959. Pigeon Point Formation of Late Cretaceous age, San Mateo County, California. *Bull. Am. Ass. Petrol. Geol.* **43**, 2855–2865.

Holst, T. B. 1982. The role of initial fabric on strain determination from deformed ellipsoidal objects. *Tectonophysics* **82**, 329–350.

Howell, D. G. & Joyce, J. E. 1981. Field guide to the Upper Cretaceous Pigeon Point Formation. In: *Upper Cretaceous and*

Paleocene Turbidites, Central California Coast (edited by Frizzell, V.). *Pacific Coast Sect. Soc. econ. Paleont. Miner. Field Trip* **6**, 61–70.

Ingersoll, R. V. 1979. Evolution of the Late Cretaceous forearc basin, northern and central California. *Bull. geol. Soc. Am.* **90**, 813–826.

Joyce, J. E. 1981. A deformational history of the Pigeon Point Formation. In: *Upper Cretaceous and Paleocene Turbidites, Central California Coast* (edited by Frizzell, V.). *Pacific Coast Sect. Soc. econom. Paleont. Miner. Field Trip* **6**, 57–61.

Knipe, R. J. 1986. Deformation mechanism path diagrams for sediments undergoing lithification. In: *Structrual Fabrics in Deep Sea Drilling Project Cores From Forearcs. Mem. geol. Soc. Am.* **166**, 151–160.

Kulm, L. D., von Huene, R., Duncan, J. R., Ingle, J. C., Kling, S. A. Jr., Musich, L. F., Piper, D. J. W., Pratt, R. M., Schrader, H. J., Weser, O. F. & Wise, S. W. Jr. 1973. *Initial Reports of the Deep Sea Drilling Project*, 18. Washington. U.S. Government Printing Office, Washington, 97–168.

Lisle, R. J. 1977. Clastic grain shape and orientation in relation to cleavage from the Aberystwyth Grits, Wales. *Tectonophysics* **39**, 381–395.

Lisle, R. J. 1985. *Geological Strain Analysis: A Manual for the R_f/ϕ Technique*. Pergamon Press, Oxford.

Lundberg, N. & Moore, J. C. 1986. Macroscopic structural features in Deep Sea Drilling Project cores from forearc regions. In: *Structural Fabrics in Deep Sea Drilling Project Cores From Forearcs. Mem. geol. Soc. Am.* **166**, 13–44.

Matthews, P. E., Bond, R. A. B. & Van Den Berg, J. J. 1974. An algebraic method of strain analysis using elliptical markers. *Tectonophysics* **24**, 31–67.

Miller, D. M. & Oertel, G. 1979. Strain determinations from measurement of pebble shapes: a modification. *Tectonophysics* **55**, T11–T13.

Oertel, G. 1970. Deformation of a slaty, lapillar tuff in the Lake District, England. *Bull. geol. Soc. Am.* **81**, 1173–1188.

Oertel, G. 1981. Strain estimation from scattered observations in an inhomogeneously deformed domain of rocks. *Tectonophysics* **77**, 133–150.

Paterson, S. R. & Tobisch, O. T. 1993. Pre-lithification structures, deformation mechanism, and fabric ellipsoids in slumped turbidites from the Pigeon Point Formation, California. *Tectonophysics* **222**, 135–149.

Ramsay, J. G. 1967. *Folding and Fracturing of Rocks*. McGraw Hill, New York.

Ramsay, J. G. & Huber, M. I. 1987. *Techniques of Modern Structural Geology, Volume 2: Folds and Fractures*. Academic Press, London.

Seymour, S. E. & Boulter, C. A. 1979. Tests of computerized strain analysis methods by the analysis of simulated deformation of natural unstrained sedimentary fabrics. *Tectonophysics* **58**, 221–236.

Shimamoto, T. & Ikeda, Y. 1976. A simple algebraic method for strain estimation from deformed ellipsoidal objects. 1, Basic theory. *Tectonophysics* **36**, 315–337.

Tobisch, O. T. 1984. Development of foliation and fold interference patterns produced by sedimentary processes. *Geology* **12**, 441–444.

Tobisch, O. T., Fiske, R. S., Sacks, S. & Taniguchi, D. 1977. Strain in metamorphosed volcaniclastic rocks and its bearing on the evolution of orogenic belts. *Bull. geol. Soc. Am.* **88**, 23–40.

Tyler, J. H. 1972. Pigeon Point Formation, an Upper Cretaceous shoreline succession, central California coast. *J. sedim. Petrol.* **42**, 537–557.

Wentworth, C. M. 1960. Sedimentary structures and inferred turbidity current origin of the Cretaceous Pigeon Point Formation, San Mateo County, California. Unpublished M.S. thesis, Stanford University.

Wheeler, J. 1986. Strain analysis in rocks with pretectonic fabrics. *J. Struct. Geol.* **8**, 887–898.

Yu, H. & Paterson, S. R. 1991. The role of primary fabrics in sandstones on strain determinations. *Geol. Soc. Am. Abs. w. Prog.* **23**, 112.